RAPID CHANGES OF ELECTRON ACCELERATION CHARACTERISTICS AT THE END OF THE IMPULSIVE PHASE OF AN X-CLASS SOLAR FLARE

Alexander Warmuth[1], Gordon D. Holman[2], Brian R. Dennis[2], Gottfried Mann[1], Henry Aurass[1], and Ryan O. Milligan[2]
[1] Astrophysikalisches Institut Potsdam, An der Sternwarte 16, D 14482 Potsdam, Germany
[2] Laboratory for Astronomy and Solar Physics, NASA Goddard Space Flight Center, Code 682, Greenbelt, MD 20771, USA

ABSTRACT

We present a detailed spectral analysis of the X1.3 flare of 2005 January 19 using hard X-ray (HXR) spectra obtained with *RHESSI*. This flare exhibits HXR pulses during the impulsive phase, with a particularly pronounced peak at the end of the impulsive phase. This peak is associated with HXR emission up to high energies (>300 keV) but does not show any Neupert effect (i.e., no simultaneous rise in soft X-rays). Fitting the spatially integrated photon spectra with a Maxwellian plus a nonthermal thick-target component reveals that the data are consistent with a high low-energy cutoff (≈ 100 keV) of the energetic electrons during the late peak. The high low-energy cutoff straightforwardly explains the lack of a Neupert effect—while highly energetic electrons are produced efficiently, there is a lack of low-energy electrons that usually contain the bulk of the total energy. Hence, the energy input into the chromosphere remains too small to trigger chromospheric evaporation. This observation shows that the characteristics of electron acceleration can change dramatically and rapidly at the end of the impulsive phase of solar flares. This could be evidence for physically distinct acceleration processes acting in the same event, or alternatively for a sudden shift in the characteristic parameters of the accelerator. Using radio observations and comparing HXR images with magnetograms, we conclude that changes in the strength and the topology of the magnetic field in which the accelerator is working are responsible for the profound changes in the injected electron spectrum.

Key words: Sun: flares – Sun: radio radiation – Sun: X-rays, gamma rays

Online-only material: color figure

1. INTRODUCTION

Hard X-ray (HXR) observations provide the most direct diagnostics of energy release and electron acceleration in solar flares. The *Reuven Ramaty High Energy Solar Spectroscopic Imager* (*RHESSI*; Lin et al. 2002) has significantly advanced our knowledge in this spectral domain, primarily due to its high spectral resolution and simultaneous imaging capability. With *RHESSI*, it is possible to cleanly separate the thermal plasma emission from the power-law component generated by nonthermal electrons. The parameters deduced from spectral fits can be used to constrain electron acceleration models. However, a viable acceleration model must not only be able to reproduce the electron distribution for a single time interval, it must also be consistent with the characteristic temporal evolution of the injected electron flux.

The two most important temporal aspects of solar flare HXR emission are the Neupert effect and the correlation between nonthermal flux and spectral index. During the impulsive phase of flares, the soft X-ray (SXR) emission tends to resemble the time integral of the HXR flux. This relation is known as the Neupert effect (Hudson 1991) and is interpreted as a causal relationship between the injected nonthermal electrons, which generate the HXR emission, and the thermal plasma responsible for the SXR emission. In particular, the Neupert effect is taken as evidence that the injected electrons are the main driver of chromospheric evaporation. Recently, Veronig et al. (2005) have shown quantitatively that this scenario is valid, provided that the low-energy cutoff of the energetic electron flux is allowed to vary by some 10 keV.

The second characteristic temporal behavior of the HXR spectrum is the correlation between the nonthermal flux and the spectral index. In this respect, solar flares show two types of behavior: the soft–hard–soft (SHS) regime, which refers to an anticorrelation between flux at a certain energy and spectral index (i.e., higher flux is associated with a harder spectrum), is observed in nearly all emission peaks during the impulsive phase (see Grigis & Benz 2004). On the other hand, the soft–hard–harder (SHH) behavior is characterized by a progressive hardening of the spectrum, typically in the late or gradual phase of a flare (Grigis & Benz 2008). The characteristic behavior has been mainly studied for the HXR photon spectrum, but it should also hold for the injected electron spectrum, which has been verified by Warmuth et al. (2009).

Besides characterizing the typical temporal evolution of solar flares, it is also instructive to study events which violate some of the modes of behavior described above. In this paper, we analyze the X1.3 flare of 2005 January 19, which shows a particularly intriguing temporal behavior: in addition to SHS in the impulsive phase and SHH in the late phase, there is a large HXR peak at the end of the impulsive phase that does not show any Neupert effect and has unusual spectral characteristics. We report these observations in Section 2 and discuss the results of our analysis in Section 3. Our conclusions are given in Section 4. Note that Grigis & Benz (2008) have studied the correlation between flux and spectral index for this event. However, while they have focused on photon spectra, we consider the injected electron spectra.

2. OBSERVATIONS

This study focuses on the X1.3 flare that started at 08:03 UT on 2005 January 19, for which we have obtained a timeseries of *RHESSI* spectra with time bins of 20 s. For energies below

50 keV, the background was taken from the nighttime interval after 09:03 UT, while for higher energies, a linear interpolation between the time intervals before and after the impulsive phase (where there is no emission form the flare) was used. The assumed photon spectra were folded through the full detector response matrix, and corrected for decimation, pulse pileup (Smith et al. 2002), gain offset and photospheric albedo (Kontar et al. 2006). Using only a single detector for accumulating the spectra allowed us to use the advanced correction methods for pileup and gain offset provided by the OSPEX software package of the *RHESSI* analysis tools. The results shown in this paper were obtained from detector 4, which has the best energy resolution and should therefore reveal all the features in the flare spectra most clearly. In order to check our results, we have also conducted our whole analysis using detector 1, which has the highest sensitivity and good energy resolution. Finally, we also used the sum of all detectors (with exception of the problematic detectors 2 and 7) and applied the standard correction procedures which have been used in most previous studies involving *RHESSI* data. Both data sets have independently confirmed the results obtained with detector 4.

Spectral models of an isothermal component derived from CHIANTI (Landi et al. 2006) with coronal abundances and a Mazzotta et al. (1998) ionization balance, plus a nonthermal thick-target bremsstrahlung component (Brown 1971) using the Haug cross section (Haug 1997) were forward-fitted to the count rate spectra (compare with Holman et al. 2003). The spectra were fitted from 6 keV up to the energy at which the flare flux equaled the background flux, but not to energies above 300 keV. Most of the event was observed in attenuator state A3, while before 08:04 and after 08:39 UT, attenuator state A1 was present.

We checked the spatial evolution of the HXR emission with CLEAN images made using detectors 3–8 and uniform weighting, with a cadence of 20 s. The energy bands used were 6–12 keV (thermal emission) and 50–100 keV (purely nonthermal). Imaging spectroscopy was used to verify the results of the spatially integrated spectroscopy for selected time intervals. The location and motion of the HXR footpoints were compared with a *Solar and Heliospheric Observatory*(*SOHO*)/ MDI (Scherrer et al. 1995) magnetogram obtained at 08:03 UT.

As a complementary data source, we used dynamic radiospectra provided by the Potsdam-Tremsdorf radiospectrograph (Mann et al. 1992). This instrument covers the decimetric–metric regime from 40 to 800 MHz with a temporal resolution of 0.1 s.

3. RESULTS

Figure 1 shows the HXR light curves and the time history of the spectral fit results. The high-energy cutoff was not fitted since it is usually masked by the background. Individual photon spectra for three time intervals are shown in Figure 2 (these time intervals are shown as dotted vertical lines in Figure 1). Note that the vertical discontinuities in the light curves in Figure 1 are artifacts due to changes of the attenuator and decimation states.

At flare onset, only a thermal component is visible in the spectra. EM and T are already enhanced due to a previous M7.4 flare from the same AR. At 08:04 UT, a steep power-law component becomes visible. This can be clearly seen in the photon spectrum shown at the top of Figure 2. With the onset of the nonthermal electron injection, chromospheric evaporation is triggered, and EM and T start to rise. As commonly observed, using *GOES* data for determining the thermal parameters (White
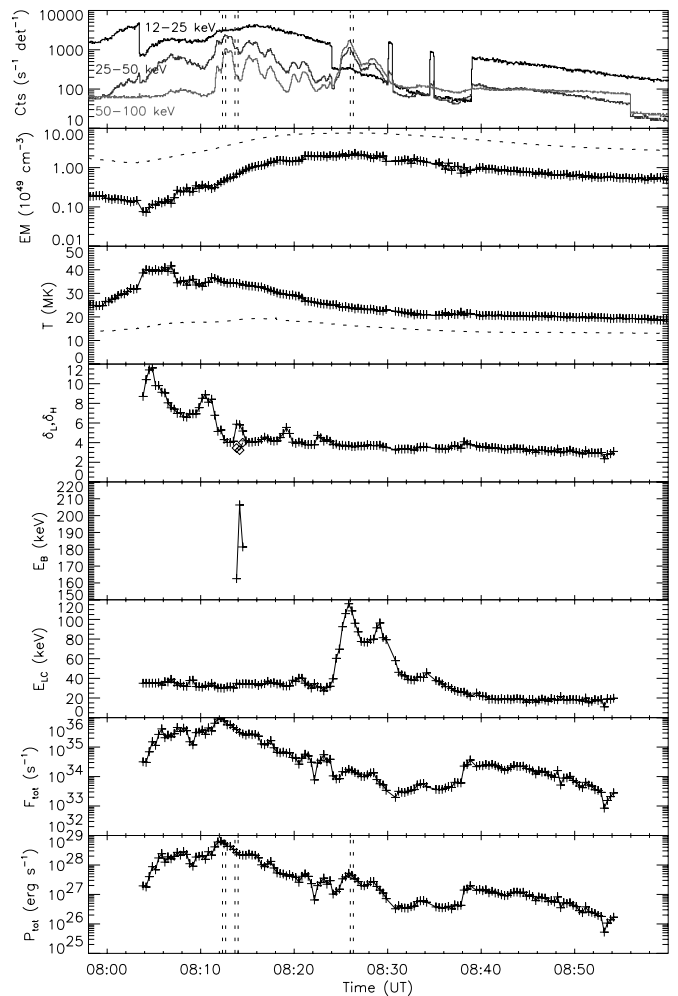
Figure 1. *RHESSI* HXR light curves and time series of fit parameters for the X1.3 flare of 2005 January 19. Shown are count rates (in counts per second and detector) in the energy bands 12–25 (black), 25–50 (gray), and 50–100 keV (light gray), emission measure EM and temperature T of the thermal plasma (crosses represent values deduced from HXR spectra, while the dotted curves are derived from *GOES* data), power-law indices of the injected electron flux below and above the spectral breaks, δ_L and δ_H (denoted by crosses and diamonds, respectively), break energy E_B, low-energy cutoff E_{LC}, total flux F_{tot} and total kinetic power P_{tot} (both integrated over all energies above the low-energy cutoff) of the injected nonthermal electrons.

et al. 2005) yield higher EM and a lower T than given by *RHESSI* (see Figure 1). Apart from issues of calibration, this may be a sign of a multithermal plasma—since *RHESSI* is sensitive to more energetic radiation, it tends to obtain higher temperatures than *GOES*.

During the impulsive phase (08:05–08:24 UT), the HXR light curves show distinct pulses at nonthermal energies with durations of 2–3 minutes. Ofman & Sui (2006) and Nakariakov et al. (2006) have interpreted these pulses as signatures of oscillations of the coronal magnetic field structures. The spectral behavior of the HXR-emitting electrons is consistent with SHS—the spectral index δ has local minima during the HXR peaks, and the total electron flux F_{tot} shows corresponding—albeit less pronounced—peaks. During this phase, the low energy cutoff lies between 30 and 40 keV and does not vary in a systematic manner. Note these values are only an upper limit for the low-energy cutoff, since the true cutoff is masked by the thermal emission (compare with Sui et al. 2005). Consequently, the derived F_{tot} and P_{tot} are only lower limits.
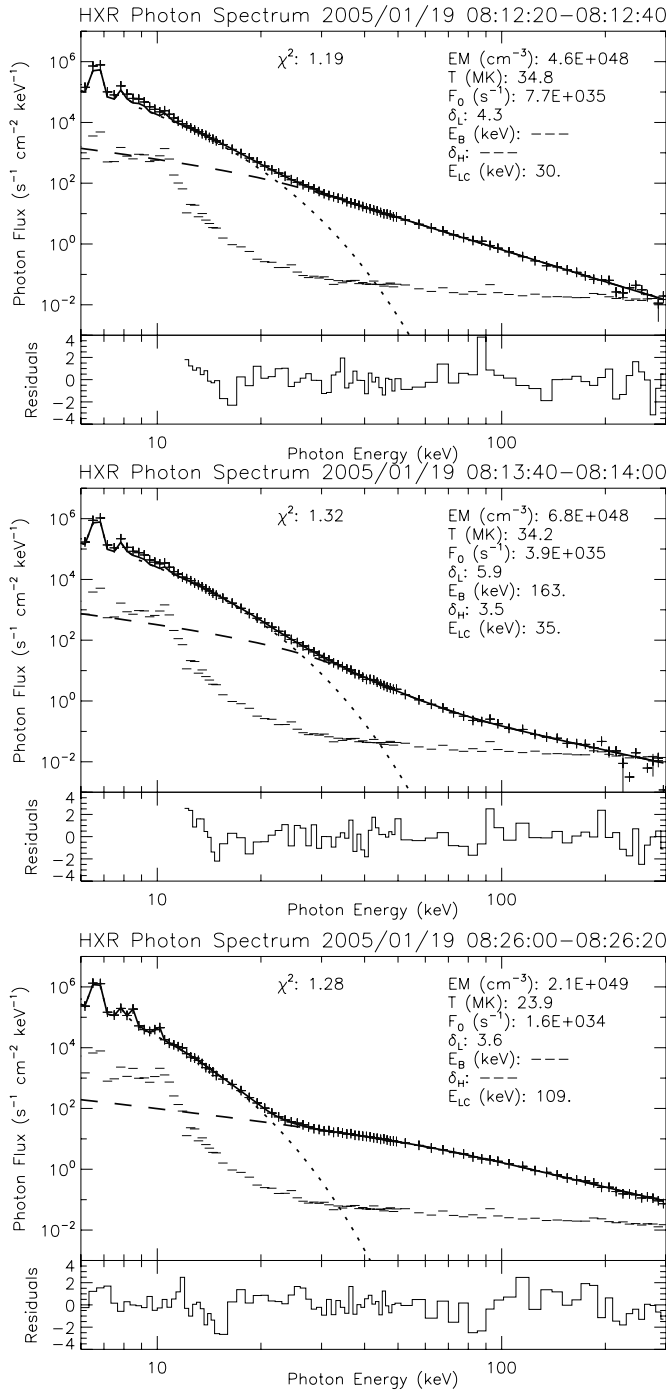
Figure 2. *RHESSI* HXR photon spectra from time intervals corresponding to the first impulsive HXR peak (top), the minimum between the first two main HXR pulses (middle), and the maximum of the late peak (bottom). The background-subtracted photon flux (plus signs; the background is shown by the horizontal bars) is plotted as a function of photon energy and is fitted with a thermal bremsstrahlung contribution from an isothermal plasma (dotted curve) and a single power-law nonthermal electron flux component with a low-energy cutoff (dashed line). The best-fit parameters and the reduced χ^2 values are shown in the plots. The normalized residuals are shown in the lower panel of each plot.

A single electron power law is consistent with the spectra for the whole period of nonthermal emission, with one exception: during the minimum between the first two main HXR pulses (around 08:14 UT), the spectra show an upward break at higher energies (i.e., $\delta_L > \delta_H$, $E_B \approx 180$ keV), as illustrated in the middle of Figure 2. This is highly unusual, since normally the

nonthermal component becomes steeper at higher energies. In large events, upward turns have been observed, but only at higher energies of several 100 keV (Dennis 1988). The only similar observation we are aware of has been reported by Dulk et al. (1992). A flattening at higher energies could be an artifact of an erroneous background estimation. However, we were able to verify the physical reality of the upward break by imaging spectroscopy, where background is not an issue, since spatially uniform background counts do not contribute to the *RHESSI* images. The effect may also be present in the other HXR minima, but there the count rate is not sufficient to draw a definite conclusion. One possible interpretation of this behavior is that there are actually two distinct electron populations: a high-flux component with a softer spectrum—this is the one which is usually observed and which shows SHS behavior— and a harder low-flux component which only becomes visible during the minima between the HXR pulses. Note that based on timing studies, Aschwanden et al. (1997) have concluded that the slowly varying HXR component which dominates between the impulsive peaks is due to a trapped electron component. Further investigation will have to show if such a harder component is actually unusual or if it is only difficult to observe because of its comparatively low flux. In any case, the presence of a second injected electron component would be evidence for distinct acceleration processes.

At the end of the impulsive phase, there is a particularly strong peak in the nonthermal HXR emission (at 08:24–08:30 UT). This late peak is actually the strongest of all HXR pulses above 40 keV, which is quite uncommon. In addition, its relation to the *GOES* SXR flux is peculiar. Whereas the SXR emission increases in accordance with the Neupert effect during the earlier pulses, it reaches its maximum at 08:24 UT, just at the onset of the late peak. During the peak, the SXR flux slowly decreases, in violation of the Neupert effect.

Let us study this behavior in more detail in terms of the evolution of the emission measure and temperature of the thermal plasma. Figure 3 shows the emission measure as deduced from *GOES* SXR observations, EM_{SXR}, the time derivative of EM_{SXR}, and the temperature of the SXR-emitting plasma, T_{SXR}. Here, we consider SXR-derived quantities because *GOES* has a broader temperature response and is more sensitive to thermal radiation of cooler plasmas. Figure 3 shows that initially EM_{SXR} increases rather gradually, but then the evaporation rate rises and $d(EM_{SXR})/dt$ reaches a maximum at 08:15 UT, after which it rapidly decreases. T_{SXR} closely follows the behavior of $d(EM_{SXR})/dt$ and starts to decrease steadily after 08:16 UT. The peaks of $d(EM_{SXR})/dt$ and T_{SXR} occur during the early nonthermal HXR pulses, an observation which can be straightforwardly interpreted in terms of electron beams driving chromospheric evaporation. A high flux of energetic electrons will result both in a high rate of evaporation and in a high temperature of the evaporated material.

During the time of the late peak (08:24-08:30 UT), $d(EM_{SXR})/dt$ has become small, and is even negative after 08:26 UT. In this respect, the late peak contrasts strongly with the earlier ones. The leveling off and beginning decrease of EM_{SXR} can be interpreted as a consequence of a significant reduction of the evaporation rate. Another possibility would be that the rather constant EM_{SXR} between 08:24 and 08:28 UT is the result of a balance between newly evaporated plasma associated with the late HXR peak and the previously evaporated material that is cooling out of the *GOES* temperature range and thus decreases in EM. However, newly evaporated material would have to be
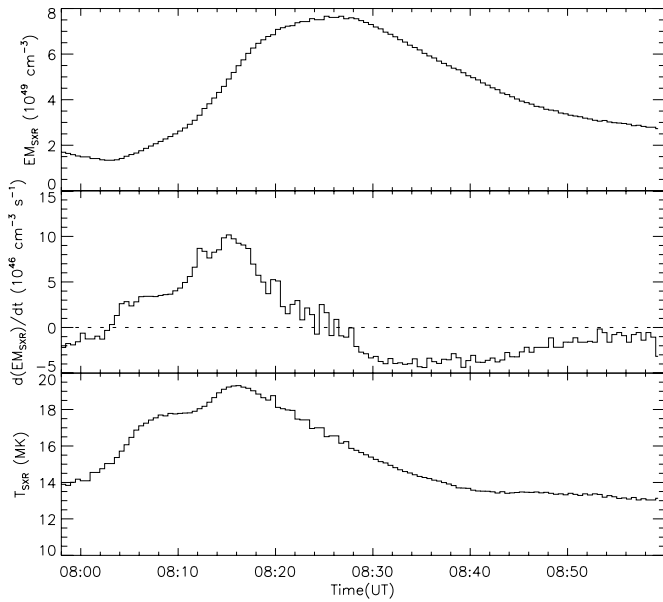
Figure 3. Temporal evolution of emission measure EM_{SXR} (top), derivative of the emission measure $d(EM_{SXR})/dt$ (middle), and temperature T_{SXR} (bottom), all derived from *GOES* SXR data. The original data with a cadence of 3 s has been rebinned to 30 s.

Figure 4. Top: background-subtracted dynamic radio spectrum (Tremsdorf radiospectrograph) showing the metric–decimetric emission of the 2005 January 19 flare. Bottom: *RHESSI* HXR count rates in the energy bands 12-25 (green), 25–50 (turquoise), 50–100 (yellow), and 100–300 keV (red).

(A color version of this figure is available in the online journal.)

significantly hotter, and we should be able to see a reduction in the rate of temperature decrease, which is not the case. This signal would be even stronger for the HXR-derived temperature, since *RHESSI* is more sensitive to high-temperature plasmas, but Figure 1 does not show any evidence for such a scenario. We conclude that despite very intense nonthermal HXR emission, chromospheric evaporation during the late HXR peak has dropped to an insignificant level when compared to the earlier peaks. The very slight increase in EM during the first half of the late peak could be due to residual evaporation which is driven/sustained by thermal conduction fronts, generated by the steep temperature gradients along the flaring loop. In any case, the sharp drop in the evaporation rate implies a corresponding dramatic reduction of nonthermal energy input.

The observed violation of the Neupert effect can be explained when we consider the results of the HXR spectral fits. While an upper limit of $E_{LC} \leqslant 40$ keV is found during both the impulsive and the gradual phases, it abruptly increases to values of up to 100 keV during the late peak (compare with Figure 1). These values are no longer just upper limits, since a break in the photon spectrum is evident well above the energies dominated by thermal emission (compare with Sui et al. 2007). This is illustrated in Figure 2: at the top, a photon spectrum from the first impulsive HXR peak is shown. The nonthermal part of the spectrum is straight on this log–log plot, which translates to a single electron power law with an upper limit for E_{LC}. In contrast, the plot at the bottom shows the spectrum from the maximum of the late peak. Here, a break in the photon spectrum is evident around 60 keV and the nonthermal spectrum below the break is very flat. This can be produced by an electron power law spectrum with a cutoff at 109 keV.

The high E_{LC} implies a low total electron flux and power— F_{tot} at the late peak is only $\approx 2\%$ of the value during the first impulsive pulse, even though the nonthermal HXR emission above 40 keV is more intense during the late peak (compare with Figure 2). This straightforwardly explains the lack of an increase in the SXR emission that would result from the chromospheric evaporation induced by the nonthermal electrons.

It is well known that forward-fitting of spectra does not yield a unique solution. In the case of the late peak, the photon spectra can be reproduced equally well by a broken electron power law which is very flat at low energies, say with $\delta_L \approx 2$, $\delta_H \approx 4$, and $E_B \approx 200$ keV. In this scenario, E_{LC} stays in the range of 30–40 keV, however, due to the fact that the electron power law is flat at low energies, the total electron flux increases by a factor of only 2–3 as compared to the case of a single power law with a high E_{LC}. The gain in kinetic power is even lower. These values would still be low enough to explain the lack of observable chromospheric evaporation.

Both possibilities discussed above imply a relative lack of low-energy electrons as compared to the other HXR pulses. This could be due to a different acceleration process becoming active, or due to a sudden shift in the characteristic parameters of the same accelerator. However, the behavior of the footpoints does not change significantly at the onset of the late peak, thus a possible second accelerator would have to be present very close to or cospatial with the main accelerator. Note that Dauphin et al. (2006) have reported an event with a somewhat similar late HXR peak. They suggest that the late peak is due to a second stage of acceleration associated with the current sheet behind an erupting flux rope.

Based on HXR observations alone, it is impossible to determine the physical reason for the sudden change in the injected spectrum. However, energetic electrons can also generate radio emission, which can be used as an independent diagnostic tool. Figure 4 shows the dynamic radiospectrum from 40 to 800 MHz (as observed by the Tremsdorf radiospectrograph) in comparison to the *RHESSI* HXR count rate in various energy bands. During the impulsive phase, we see standard flare signatures: a type II burst starting at 08:14:20 UT at frequencies around 100 and 200 MHz, and complex type IV emission between 200 and 400 MHz from 08:06 to 08:23 UT. There are four fast drift pulsating features in the type IV burst which are correlated in time with the earlier HXR pulses around 08:08, 08:13 (this is the main HXR pulse), 08:18, and 08:20 UT. The second to fourth pulses are similar to drifting decimetric chains (Karlický et al. 2004).

With the onset of the late HXR peak, the radio spectral features change dramatically. Between 08:25 and 08:27 UT, a diffuse broadband continuum grows in intensity from 800 MHz
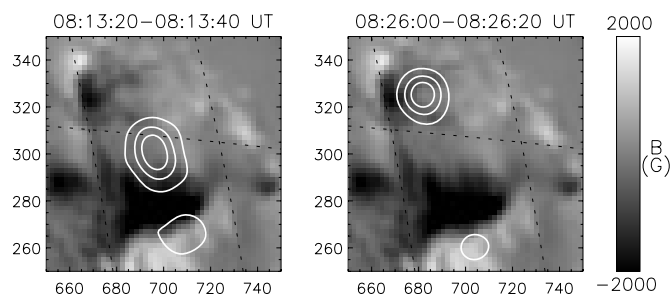
Figure 5. *RHESSI* CLEAN HXR images in the energy band 50–100 keV (white contours) overplotted on an MDI magnetogram (grayscale). Contour levels are at 25%, 50%, and 75%. For details see the main text.

down to at most 200 MHz (due to data quality, it is difficult to say if the emission at lower frequencies also belongs to this continuum) and decays slowly until 08:35 UT. While the diffuse emission continues after the late HXR peak, its most intense part is restricted to the duration of the HXR pulse.

It is generally believed that such smooth continua are due to gyrosynchrotron emission of mildly relativistic electrons in coronal magnetic fields (Bastian et al. 1998). The temporal profile of the emission—fast rise and much slower decay—suggests that radio-emitting electrons are injected into a coronal magnetic trap that results from the convergence of field lines in the transition region and chromosphere. Subsequently, they precipitate out of the trap on timescales of minutes, giving the slow decay of the gyrosynchrotron radiation. However, since trapping is only weakly dependent on energy, it cannot account for the reduction of the flux of low-energy electrons during the late peak—we still need a change in the acceleration itself.

One hint at changes in the characteristics of the accelerator is given by the sudden onset of the gyrosynchrotron emission. This implies that electrons are now injected into fields with a different topology than before, namely strongly converging ones to produce a trap. At the same time, the strong gyrosynchrotron emission requires high magnetic field strengths, which also points to a significantly changed magnetic field configuration in which the accelerator is working. This scenario is supported by the characteristics and the evolution of the HXR footpoint sources. Figure 5 shows the nonthermal footpoints for the early peak of the impulsive phase (left) and the maximum of the late peak (right). They are overplotted on an MDI magnetogram. Throughout the event, the southern footpoint is smaller and fainter than the northern one, which implies stronger mirroring in the south. While this footpoint remains close to the neutral line, the northern one moves further northeast. At the time of the late HXR pulse, it has reached a region of higher field strengths, with a mean B of $\approx$600 G when integrated over the 50% contour of the footpoint. The region of higher field strength can be seen as the dark patch in the northeast part of Figure 5 (right). For comparison, before the footpoint has approached this region, the mean field strengths are in the range of 200–300 G.

The spatial association of the footpoint with the northeastern region implies that particles are now accelerated in a distinct magnetic structure. Provided that these fields are strongly converging, this could close the northern footpoint of the magnetic trap, allowing for an accumulation of energetic electrons in the corona and explaining the onset of gyrosynchrotron emission.

4. CONCLUSIONS

At first sight, the X-class flare of 2005 January 19 shows the typical characteristics of high-energy spectral evolution—

the Neupert effect is present, the impulsive phase shows soft–hard–soft HXR spectral evolution, while the gradual phase is dominated by soft–hard–harder behavior. However, there is a period where some of these typical characteristics are violated: a particularly intense HXR peak at the end of the impulsive phase does not show any association with an increase of the SXR flux. Fitting thick-target electron spectra to the observed spectra, we were able to show that this discrepancy can be explained by the characteristics of the injected electron flux. Despite the high HXR photon flux during the late peak, the total flux (and power) of the injected electrons was lower than during the earlier peaks by more than an order of magnitude, which apparently was too low to drive detectable chromospheric evaporation.

Based on the spectral analysis, the low electron flux during the late HXR peak can be explained either by a high low-energy cutoff of a single electron power-law spectrum or by a broken power-law with a low spectral index below the break energy. Either case implies a relative lack of low-energy (i.e., tens of keV) electrons as compared to an unbroken power law extending to low energies. This suggests that either a second acceleration mechanism is working during the late peak, or that the characteristic parameters of the accelerator suddenly changed. The sudden onset of gyrosynchrotron emission, which is in temporal agreement with the rise of the late HXR peak, suggests that accelerated electrons are injected into a magnetic field configuration which acts as a trap. At the same time, the northern HXR footpoint reaches a region of high field strength. Thus, we have evidence that during the late HXR peak both the strength and the topology of the magnetic field structures in which the accelerator is working are changing. Since the magnetic field is the most important ingredient in any acceleration mechanism and the ultimate source of all the energy, it is not unreasonable to expect that drastic changes in the field will lead to a profound variation in the accelerated electron spectrum. Thus, it is entirely possible that the same basic mechanism is responsible for electron acceleration during the whole event.

REFERENCES

Aschwanden, M. J., Bynum, R. M., Kosugi, T., Hudson, H. S., & Schwartz, R. A. 1997, ApJ, 487, 936
Bastian, T. S., Benz, A. O., & Gary, D. E. 1998, ARA&A, 36, 131
Brown, J. C. 1971, Sol. Phys., 18, 489
Dauphin, C., Vilmer, N., & Krucker, S. 2006, A&A, 455, 339
Dennis, B. R. 1988, Sol. Phys., 118, 49
Dulk, G. A., Kiplinger, A. L., & Winglee, R. M. 1992, ApJ, 389, 756
Grigis, P. C., & Benz, A. O. 2004, A&A, 426, 1093
Grigis, P. C., & Benz, A. O. 2008, ApJ, 683, 1180
Haug, E. 1997, A&A, 326, 417
Holman, G. D., Sui, L., Schwartz, R. A., & Emslie, A. G. 2003, ApJ, 595, L97
Hudson, H. S. 1991, BAAS, 23, 1064
Karlický, M., Fárník, F., & Krucker, S. 2004, A&A, 419, 365
Kontar, E. P., MacKinnon, A. L., Schwartz, R. A., & Brown, J. 2006, A&A, 446, 1157
Landi, E., Del Zanna, G., Young, P. R., Dere, K. P., Mason, H. E., & Landini, M. 2006, ApJS, 162, 261

Lin, R. P., et al. 2002, Sol. Phys., 210, 3

Mann, G., Aurass, H., Voigt, W., & Paschke, J. 1992, Proc. First SOHO Workshop: Coronal Streamers, Coronal Loops, and Coronal and Solar Wind Composition, ed. C. Mattok (ESA SP-348; Noordwijk: ESA), 129

Mazzotta, P., Mazzitelli, G., Colafrancesco, S., & Vittorio, N. 1998, A&AS, 133, 403

Nakariakov, V. M., Foullon, C., Verwichte, E., & Young, N. P. 2006, A&A, 452, 343

Ofman, L., & Sui, L. 2006, ApJ, 644, L149

Scherrer, P. H., et al. 1995, Sol. Phys., 162, 129

Smith, D. M., et al. 2002, Sol. Phys., 210, 33

Sui, L., Holman, G. D., & Dennis, B. R. 2005, ApJ, 626, 1106

Sui, L., Holman, G. D., & Dennis, B. R. 2007, ApJ, 670, 862

Veronig, A., et al. 2005, ApJ, 621, 482

Warmuth, A., Mann, G., & Aurass, H. 2009, A&A, 494, 677

White, S. M., Thomas, R. J., & Schwartz, R. A. 2005, Sol. Phys., 227, 231